

University of California
Santa Barbara

**Constraints on the Higgs boson total decay width
from off-shell production with decay into pairs of
Z-bosons in simulated data**

A dissertation submitted in partial satisfaction
of the requirements for the degree

Bachelor of Science
in
Physics

by

Jiahong (Jerry) Ling | 凌嘉鸿

Committee in charge:

Professor Claudio Campagnari, Chair
Doctor Sathya Guruswamy

June 2020

The Dissertation of Jiahong (Jerry) Ling | 凌嘉鸿 is approved.

Doctor Sathya Guruswamy

Professor Claudio Campagnari, Committee Chair

June 2020

Constraints on the Higgs boson total decay width from off-shell production with decay
into pairs of Z-bosons in simulated data

Copyright © 2020

by

Jiahong (Jerry) Ling | 凌嘉鸿

Acknowledgements

The research presented in this senior thesis would not have been possible if not many people's guidance, encouragement, and help. Foremost, I would like to thank my research adviser Dr. Claudio Campagnari for his constant support and mentorship, both in research and my student life in the past almost 3 years. He leads me into the field of high energy physics and had provided personal attention to my progress along the way. He is also the one who suggested the research topic to me as a step up from what I have been doing.

At the same time, I would also like to thank Dr. Ulascan Sarica, who is the a primary correspondent in physics analysis for this research at UCSB. It would not be possible for me to undertake such a complex analysis if not for his dedication and careful teaching.

Additionally, I would like to acknowledge the help of Nick Amin, who guided me personally in the summer of 2017 when I first joined the group. Nick has also helped me tremendously in both physics and technical issues and has provided many useful tools for physics and computing. In the same regard, I would like to thank Bennett Marsh and Sicheng Wang for their help and guidance in the past years.

Abstract

Constraints on the Higgs boson total decay width from off-shell production with decay into pairs of Z-bosons in simulated data

by

Jiahong (Jerry) Ling | 凌嘉鸿

The discovery of the Standard Model (SM) Higgs boson at the Large Hadron Collider (LHC) was a major achievement of the experimental particle physics community in the 21st century. Though a fair portion of the physics analysis focus has shifted to Supersymmetry (SUSY) physics, the direct search of SUSY models has yield null results so far. Meanwhile, many properties of the Higgs boson are still to be measured.

In this analysis, we present constraints on the total decay width of Higgs boson, Γ_H , by using the on-shell and off-shell decay rates of Higgs boson to a pair of Z bosons with one Z-boson decaying into a pair of electrons or muons and the other into neutrinos. A total number of 2 (ee or $\mu\mu$) \times 4 ($N_{\text{jets}} = 0, 1, 2, 3+$) $= 8$ channels are considered and used for limits fitting. The result represents the expected constraints using the physics events and CMS experiment detector response simulated data via Monte Carlo methods (MC). The data and expected results correspond to data collected in 2016, 2017, and 2018, which has an integrated luminosity of 137.15 fb^{-1} at a center-of-mass energy of 13 TeV. The expected constraint based on simulation is $\Gamma_H < 16.4 \text{ MeV}$ 95% CL.

Contents

Abstract	v
1 Introduction	1
1.1 Physics at the LHC (and elsewhere)	1
1.2 The CMS Detector	2
1.3 The Higgs boson and off-shell methods	5
1.4 Background and signal simulation	7
1.5 Uncertainties	10
2 Methods	11
2.1 Event selection and physical variables	11
2.2 Signal samples re-weighting	15
2.3 Strategy in variable selection and binning and systematical uncertainties	20
3 Results and interpretation	23
3.1 Limits on Higgs decay width	24
A Weights table for Higgs sample	26
A.1 Windowed re-weighting results	26
A.2 Sample mass factors for ggZZ and VBF_ZZ samples	27
B Additional figures	29
B.1 1D Histograms of variables used for constructing 2d templates histograms	30
B.2 Signal sample fitting template histogram of background and signal (z-axis scaled by 1×10^5)	30
B.3 Signal sample fitting template histogram relative error of background and signal	36
Bibliography	40

Chapter 1

Introduction

This chapter contains a brief introduction of the experimental aspect of the Large Hadron Collider (LHC) physics, the Compact Muon Solenoid (CMS) detector, and the physics behind the off-shell methods for constraining the Higgs decay width. Finally, we also present a very brief technical account for the Monte Carlo (MC) events production.

1.1 Physics at the LHC (and elsewhere)

After the discovery of standard model (SM) Higgs boson in 2012, the LHC went through a series of upgrades during 2013–2015 and finally restarted with center-of-mass energy reaching 13 TeV. Though the last particle promised by the SM has been discovered, there remains ‘known’ mysteries in high energy physics.

Although the SM is one of the most precise theories in physics we ever had, the model requires many ‘inputs’ from the experiment for parametrization, and cannot account for phenomena such as neutrino oscillation with its original form. One proposed (and admittedly the most popular one) solution is called Supersymmetry (SUSY), which is one of the many models under the boarder term beyond-the-standard-model (BSM) physics.

SUSY predicts the existence of more particles than what we have identified so far in the SM. Because these predicted particles have a ‘mirror’ extension/association to the SM particles, they are often addressed as SUSY partners (as each fundamental fermion in the SM would have a bosonic SUSY partner and vice versa). While the direct searches for these SUSY partners in the past few years have all yielded null results, they have not discouraged physicists from other attempts of probing the BSM physics in other ways.

The Higgs boson has a special role in the process mainly due to the Higgs field, from which the particle originates from. The Higgs field couples to all massive particles, thus making the Higgs boson a window to probe the BSM physics, as discussed in Section 1.3.

The LHC has been operating at the same energy for the past 3 years (2016-2018) with the delivered luminosity ramping up in each year[1]. In this analysis, we will be mostly using simulations that were produced corresponding to Run period 2018, but scaled to 137.15 fb^{-1} to simulate the expected result by using the entire Run 2 data, for the Compact Muon Solenoid (CMS) detector.

1.2 The CMS Detector

Though we are not using the data accumulated by the CMS detector, the simulated events are reconstructed based on the material interaction and electronics responses of the real detector using the GEANT4 package [2].

The defining feature of the CMS detector is the solenoid (which is what the S stands for) around the beamline, in the middle of the detector [3]. This superconducting solenoid produces a 4 T magnetic field and is 12.5 m long free bore [3]. This feature allows the tracking of charged particles by bending their trajectory when hitting various layers of the detector.

¹<https://cds.cern.ch/record/2120661>

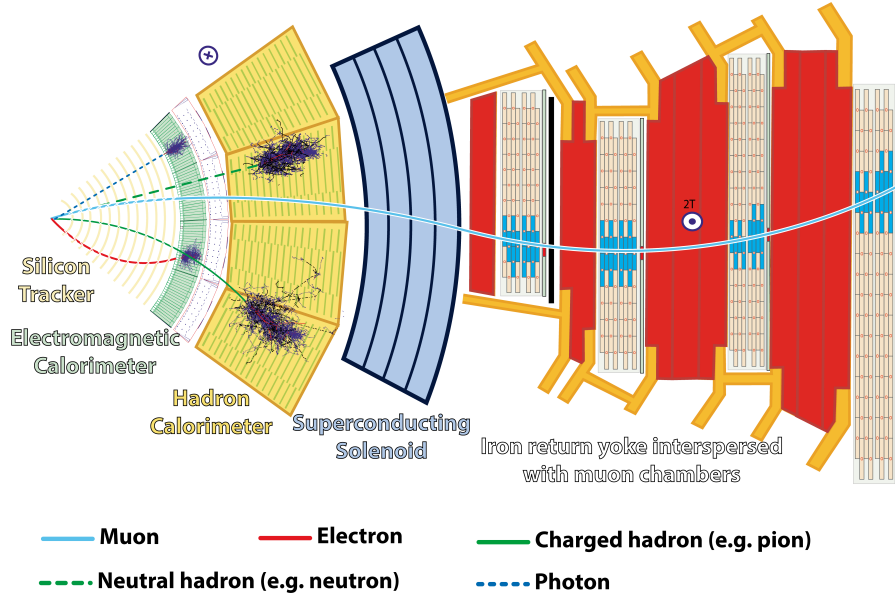


Figure 1: A section slice of the CMS detector where we can see how particles with different physical properties interact differently with the detector.¹

One important kind of ‘final-state’ particles used in this thesis is charged lepton, which includes electrons and muons (the half-life of tau-on is too short to interact with the detector directly); ‘final-state’ here means they are the end products of a decay chain and are recorded by the detector components directly. If we concentrate on the red and blue lines in Fig. 1, we can see that electrons (red) leave a few hits that resemble a curved track within the silicon tracker and are stopped at the electromagnetic calorimeter (ECAL).

For the muons (blue line in Fig. 1), they largely go through all the interior layers unhindered due to their higher mass and the fact that they only interact electromagnetically (unlike a proton, for example); pay close attention to the ‘S’-shaped curve, this is due to the opposite magnetic field outside of the superconducting solenoid. The iron return yoke also stops particles other than muons coming through (except neutrinos which always travel freely). Although information such as momentum relies on hits on the silicon

trackers, the hits in the muon chambers and a matching trajectory are needed for the object to be reconstructed as a muon. Notice how the muon chambers occupy more than half of the detector by size. Such a design allows the CMS detector to excel in muon measurements and is the primary reason for the overall design.

Zooming out from the individual components of the detector, the complete (physics object) reconstruction process is complex and sometimes requires information from multiple parts of the detector. This algorithm is called the Particle Flow (PF) [4]. While the energy of simple and neutral objects such as photon are directly measured by the ECAL (with correction such as zero-suppression, where minimal activities are treated as zero value during readout), electron measurements need the information from the inner tracker (to determine charge and momentum), energy at the ECAL, and also, the sum of the energy of photons produced by bremsstrahlung (when electron interacts with the detector material) compatible with the electron's track.

For gluons and quarks that come out of the interaction vertex, due to quark confinement, the detector is only be able to ‘see’ a narrow ‘spray’ of final state (stable) particles that subsequently are clustered into objects called ‘jets’. There are different algorithms and criteria to combine a collection of measurements into a single jet, in the CMS at the moment, the anti- k_t clustering algorithm [5, 6] is used. In short, the algorithm would cluster objects in a roughly cone-like space that originated from the vertex according to some parameters. The algorithm is resilient to QCD effects that would cause jets to split, such as shown in Fig. 2

In this analysis, we use the AK4 jets which means that the algorithm is given a $R = 0.4$ parameter. Another common choice is $R = 0.8$, which is preferred in some cases for boosted topologies due to a larger ‘opening angle’.

²https://twiki.cern.ch/twiki/bin/viewfile/Sandbox/Lecture?rev=1;filename=Philipp_Schieferdeckers_Lecture.pdf#page=3

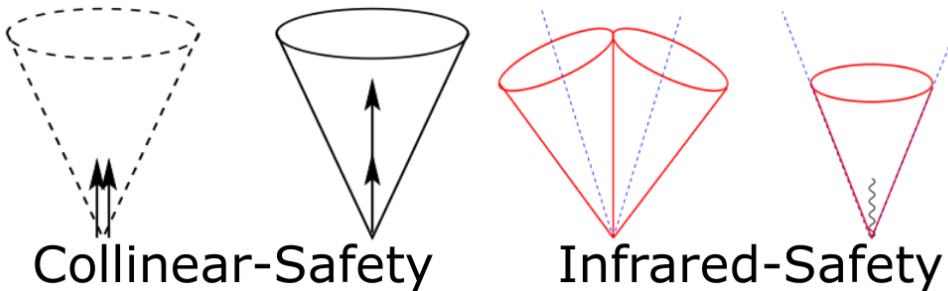


Figure 2: A illustration of two kinds of QCD effects in jets²

1.3 The Higgs boson and off-shell methods

As mentioned above, the Higgs boson has a special place as it can be seen as a ‘bridge’ between the SM and the BSM (in some models), as some SUSY particles can decay into it or decay out from it, or simply have a BSM production Feynman diagram that leads to a higher Higgs bosons production rate than the SM expects. In any of these cases, the basic properties of the SM Higgs boson remains important.

The importance of studying the Higgs also comes from the fact that it is an ‘add-on’ to the SM as a mass generation mechanism for gauge bosons and fundamental fermions. The Higgs sector of the SM is not well tested, and, in theory, could be more complicated than the minimal SM suggests. For example, multiple Higgs bosons may be present, or the observed Higgs may be a composite particle. Interestingly, if not composite, the observed Higgs boson would be the only spin-zero fundamental particle we know.

Many properties are well measured, such as its mass and spin [7]; others, however, have not entered the realm of ‘precision’ physics so far. One of them is the total decay width of the Higgs boson, which is of course associated with the particle’s half-life τ as $\Gamma = \frac{\hbar}{\tau}$. The SM predicts that the Higgs boson will have a decay width of 4.07 MeV. The problem is that the energy resolution of the CMS detector, which is around $\mathcal{O}(1)$ GeV for the di-photon or 4-leptons final states, is not even remotely close to that prediction.

One way to measure the decay width suggested by the theorists is to indirectly measure it using the off-shell method [8, 9]. When a Higgs boson decays into two massive vector bosons (VV) (in the scope of this thesis, two Z bosons), one of them has to be off-shell, or the Higgs boson is off-shell. This is because $m_H \approx 125 \text{ GeV}$ is smaller than the mass of two W-bosons ($\approx 160 \text{ GeV}$) or of two Z-bosons ($\approx 182 \text{ GeV}$). The Higgs boson decay branching ratio is coupled to the daughter particles' mass, and thus this cross-section $\sigma_{H \rightarrow VV}$ is enhanced as the mass of Higgs boson gets closer to the on-shell VV mass.

In fact, the production of Higgs boson from a pair of vector boson is also related to the decay width of Higgs boson Γ_H via the ‘propagator’[10]. In terms of the differential cross-section:

$$\frac{d\sigma_{vv \rightarrow H \rightarrow VV}}{dq_H^2} \sim \frac{g_{vvH}^2 g_{HVV}^2}{(q_H^2 - m_H^2)^2 + m_H^2 \Gamma_H^2} \quad (1)$$

where the two g on the right-hand side are the couplings for production from vv and decay to VV respectively. By integrating this equation near the on-shell mass of the SM Higgs boson or in the tail region (above the mass of a pair of V’s), one can translate the differential cross section into event rate that can be (in theory) measured in experiments:

$$\begin{aligned} N_{vv \rightarrow H \rightarrow VV^*}^{\text{on-shell}} &\sim \frac{g_{vvH}^2 g_{HVV}^2}{m_H \Gamma_H} \sim \mu_{vvH} \\ N_{vv \rightarrow H^* \rightarrow VV}^{\text{off-shell}} &\sim \frac{g_{vvH}^2 g_{HVV}^2}{(q_H^2 - m_H^2)^2} \sim \mu_{vvH} \cdot \Gamma_H \end{aligned} \quad (2)$$

The key takeaway is that, up to some correction factors, the event rate of off-shell Higgs scales linearly respect to the Higgs decay width Γ_H which allows indirect measurement of the width itself.

In this thesis, we will focus on the $H \rightarrow ZZ \rightarrow 2\ell 2\nu$ channel at the CMS detector using

simulated (MC) events. The work conducted here is part of the ongoing analysis within a group formed by the UCSB HEP group, Université Libre de Bruxelles, and Beihang University under the CMS Collaboration³. The analysis items and methods included in this thesis are a subset of what will be in the official analysis and is a part of the final measurement. More details on what approximations have been taken in order to obtain a preliminary expected result will be discussed in the next few sections.

1.4 Background and signal simulation

The following list contains the MC samples (by physical process) used in this thesis, the first two contain (off-shell) Higgs boson in the intermediate state:

- ggZZ offshell: Gluon fusion $gg \rightarrow H \rightarrow ZZ$
- VVZZ offshell: Vector boson fusion (VBF) into Higgs boson
- qqZZ, qqWZ, qqWW
- DY: Drell-Yan process
- TT: $t\bar{t}$, including samples with additional vector boson (TTW/TTZ) or photon + jets (TTGJets).

The MC samples for all processes except DY are produced in Run 2 Autumn18MiniAOD-102X analysis, DY sample is produced in Run 2 Summer16MiniAODv3 94X analysis and scaled appropriately afterward. As their names suggest, each year in the Run 2 (2016-2018) has their separate MC samples since the running condition (the LHC) and the condition of CMS can change from year to year, though the physics remains the same.

³Internally, CMS AN-20-081

Various programs are used in the long chain of simulated events production. POWHEG v2 [11], JHU GENERATOR AND MELA [12], are used for the signal simulation. MADGRAPH [13] is used to generate NLO background samples, PYTHIA [14] for parton showering and NNPDF 3.1[15] sets are used for the parton distribution functions.

Before diving into the procedure in which the signal samples are generated separately and subsequently combined via a reweighting, it would be appropriate to give an account for the general idea behind the ‘event weight’ and its significance.

As described at the beginning of this section, events that correspond to different physical processes are generated in different MC configurations at different ‘orders’ of the QCD/QED physics. Naively, one would imagine a process where the MC can directly simulate the complete physics at the LHC at a given center-of-mass energy. Unfortunately, this is neither efficient nor possible. It is not possible because some physical processes (especially QCD ones) are non-perturbative and stepped approaches are taken to gradually build-up to the final event. It is also impossibly inefficient because the processes that an analysis is concerned with (for example, in all SUSY searches) usually have a tiny (if not 0) cross-section compared to other common processes that can be found at $\sqrt{s} = 13 \text{ TeV}$ at the LHC. And it would be a waste of computing resources to generate common processes over and over again.

Example of some important weights		
Name	abbr.	Description
Generator weight	GEN wgt	Given by MC event generator
Pile-up weight	PU wgt	Correction for the pile-up effect ⁴
Matrix element weight	ME wgt	From generator that uses ME Likelihood approach
K-factor	Kfactor	Correction for LO cross section of QCD processes

Table 1: An incomplete list of weights used in the MC events used.

In reality, Monte Carlo events are each given many ‘weights’ (Tab. 1), so that we don’t have to generate uninteresting processes. At the same time, for the events that

lack in number (i.e. it results in poor statistical distribution), one can optionally generate extension events set for it. In practice, (for example as shown in Fig. 3) you can have 1×10^6 raw MC entries, but only 100 expected events (yield) in the integration of the histogram, due to the physics process being very rarely seen. But, these 1×10^6 would form a much smoother distribution than if you only had 100 entries to work with. Also, this enables the generation of ‘unknown’ processes which can be used to constrain possible new physics in a likelihood fit (against null hypothesis).

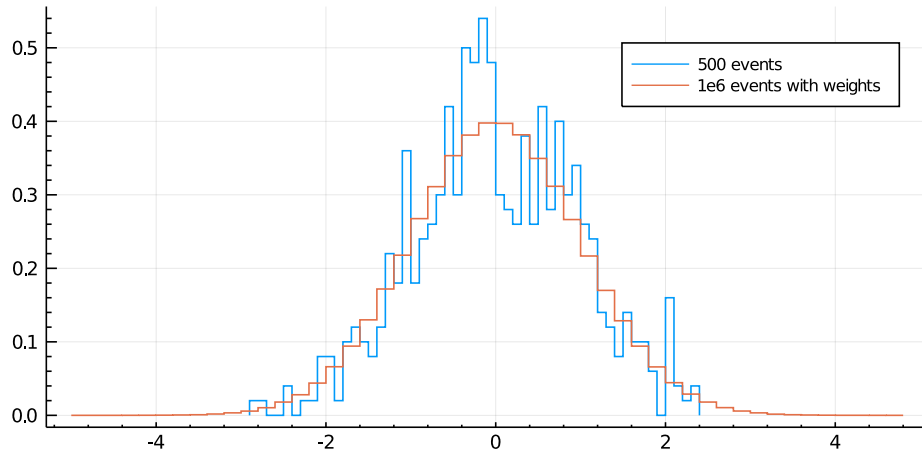


Figure 3: Illustrative plot to show how weights can make distribution smoother without altering the total number of expected events.

In this thesis, we explicitly use K-factors, and variations of it to obtain Electroweak systematical uncertainty in $\text{qqZZ}/\text{qqWZ}/\text{qqWW}$ backgrounds. For the signal processes involving the Higgs boson, special treatment is given to merging and obtaining high-statistics samples from multiple ‘raw’ samples with different pole mass of Higgs boson corresponding to the m_H term in the denominator on the right-hand side of Eq. 1. This approach is also desirable for the generation of off-shell (Higgs) decays. The procedures used and the resultant combined signal samples are discussed in the Sec. 2.2.

⁴when many unwanted collisions happen in the same bunch crossing

1.5 Uncertainties

A limited number of experimental and theoretical uncertainties in both signal and background processes are discussed here. Although dedicated to MC-only analysis, the leading theoretical uncertainties are considered:

Source	Uncertainty	Affected processes
Integrated luminosity	2.5%	ggZZ, VVZZ, qqZZ, qqWZ
Non-resonant background estimation	10%	TT, qqWW
Electroweak	1σ	qqZZ, qqWZ
Higgs branching ratio	2%	ggZZ, VVZZ
gg background	10%	ggZZ

Table 2: Summary of systematic uncertainties considered in this thesis and their magnitude as well as processes affected by them.

Most of the uncertainties are simply experimental, for example, the luminosity. The Electroweak (EW) uncertainties are obtained by scaling EW NLO K-factor up or down on the corresponding samples and non-resonant background comes from separate studies that examine e/μ events in the data, which are limited by the number of events within the Z-boson mass window. Here we approximate this uncertainty as $\pm 10\%$. The gg background uncertainty is parametric respect to the M_T^{ZZ} defined below [16, 17, 17].

Chapter 2

Methods

In this chapter, we give a description of event selection, definitions of key physical variables and how they are used to select events. Then, a procedure regarding how the signal sample is manipulated to produce a high statistics off-shell Higgs sample is presented. Finally, the binning of variables used to obtain the results are determined and defined.

2.1 Event selection and physical variables

Proton bunches cross each other at a rate of about 400 MHz in the beamline of the LHC. Naturally, not all of these crossings are recorded due to both technical limitation of the electronics as well as the fact that the vast majority of these crossings don't produce inelastic collision that is energetic enough to be interesting.

After the selection of Level 1 (L1) trigger and the higher level trigger (HLT), less than 1000 events per second are permanently recorded and go to full off-line reconstruction. Among these, we only select the ones that pass certain HLT trigger, for 2018 data set:

- HLT_Mu17_TrkIsoVVL_Mu8_TrkIsoVVL_DZ_Mass3p8
- HLT_IsoMu24

- HLT_Ele23_Ele12_CaloIdL_TrackIdL_IsoVL
- HLT_DoubleEle25_CaloIdL_MW
- HLT_DoublePhoton70
- HLT_Ele32_WPTight_Gsf
- HLT_Photon200

Most of the trigger names are self-explanatory, for example, the numbers are the transverse momentum (p_T) threshold (in GeV) to pass each of them. The HLT is the starting point of the analysis. The purpose of the triggers is to ensure that the events in the corresponding samples will contain the physics we wanted (since run data samples are divided according to what triggers they passed).

The next step is to ‘add’ composite variables that are relevant to the physics we are interested in, well as making base-line cuts on the events. The jets are all AK4 jets unless mentioned otherwise, and a special type of jets called b-tagged jets are identified using the DeepFlavour algorithm.[18] These jets likely originate from relatively long-lived bottom quarks judging based on a combination of many measurements including the displacement of vertices. We shall also define a few of the uncommon variables in the list and physical motivations are given in the following paragraphs.

After mandating passage of the set of triggers above, based on more delicate physics reasons, the baseline cuts are:

- Missing transverse energy $E_T^{\text{miss}} > 125\text{GeV}$: the signal process creates true E_T^{miss} with neutrinos, this cut also reduce bkg such as DY.
- Both leptons have $p_T > 25\text{ GeV}$
- $|\Delta\phi_{\ell\ell-E_T^{\text{miss}}}| > 1.0$

- $|\Delta\phi_{\ell\ell\text{Jets}_E_T^{\text{miss}}}| > 2.5$
- $|m_{\ell\ell} - 91.2 \text{ GeV}| < 15 \text{ GeV}$: the signal process consists of $Z \rightarrow \ell\ell$, we require the di-lepton system has a mass that is consistent within the Z mass peak.
- $p_T^{\ell\ell} > 55 \text{ GeV}$: the Drell–Yan (DY) process creates a lot of backgrounds events, but their di-leptons go back-to-back with expected value of this variable close to 0.
- No ak4-jet b-tagged jet ($\Delta R = 0.4$, loose b-tagging working point (WP))
- $\min |\Delta\phi_{j_E_T^{\text{miss}}}| > 0.25$

In addition, to reduce the detector effects at high pseudo rapidity angles:

- $\eta_\mu < 2.4$
- $\eta_e < 2.5$

First and most importantly, the E_T^{miss} cut reduces background from DY significantly, since they don't have real E_T^{miss} . Notice that many of the cuts are related to angles between various physical objects presented in the reconstruction. The reason is simple: the signal events, where Higgs goes to ZZ and one Z goes to 2 charged leptons and the other goes to 2 neutrinos, ideally would have the two Z 's momentum ‘back-to-back’ in Higgs boson's rest frame, leading to a large angle in the transverse plane.

Furthermore, in background events which do not contain this kinematic feature, the correlation in the directions of $\vec{E}_T^{\text{missing}}$ and the transverse momentum of the leptons is weaker.

To use this kinematic feature to increase the signal to background ratio, we define $|\Delta\phi_{\ell\ell_E_T^{\text{miss}}}|$ as the azimuthal angle (perpendicular to the beamline) between the di-lepton system and the transverse missing energy. In the signal events that produce 0 jets, this

variable should be π . The cut is lowered to 1.0 due to the finding that in the (not so rare) cases where there is jet(s) recoiling against the ZZ system, this variable can go quite low.

This leads to the next variable on the list, $|\Delta\phi_{\ell\ell\text{Jets}_E^{\text{miss}}}|$, which is almost the same except that we add all jets' momentum into the di-lepton system to account for the events that have produced jets, which in turn would cause the angles to be lower in a multi-body final state.

Also, a veto on the b-tagged jet is placed to reduce the background events originated from a pair of top quarks ($t\bar{t}$) since top quark always decay to a bottom quark.

Finally, $\min |\Delta\phi_{j_E^{\text{miss}}}|$ is the minimum azimuthal angle difference between any of the jet (that passes cuts) and the E_T^{miss} . The cut exists because jets are one of the most difficult physical objects to measure, they often create so-called instrumental E_T^{miss} due to jet mis-measurements and it can be quite large in magnitude. However, such mis-measurements often yield large E_T^{miss} in the direction of the original jet. This cut requires angular separation since in the signal processes, the jet recoils against the ZZ system.

We also define variables that are not cut on, but are used for fitting:

$$D_{jj}^{VBF} = \frac{P_{\text{SM}}^{VBF}(\vec{\Omega})}{P_{\text{SM}}^{gg}(\vec{\Omega}) + P_{\text{SM}}^{VBF}(\vec{\Omega})} \quad (3)$$

as first introduced in another CMS paper [19]. In short, this variable (discriminator) is sensitive to the VBF physics and the correlation between (angles and mass of) the outgoing jets resulted from the VBF topology. At the same time:

$$M_T^{\text{ZZ}} = \left[\sqrt{p_{T,\ell\ell}^2 + m_{2\ell}^2} + \sqrt{E_T^{\text{miss}}{}^2 + m_Z^2} \right]^2 - \left[\vec{p}_{\ell\ell} + \vec{E}_T^{\text{miss}} \right]^2 \quad (4)$$

is defined based on the hypothesis that the E_T^{miss} is comprised of mainly the two neutrinos

from one of the Z bosons. We shall see the usefulness of this variable in channels where not enough jets are present to construct the D_{jj}^{VBF} variable.

On top of the cuts stated in the beginning, several E_T^{miss} filters exist to remove detector anomalies. A lepton isolated track veto is implemented in the underlying analysis framework to remove events with additional leptons that are likely backgrounds, such as those can be found in WZ.

2.2 Signal samples re-weighting

Extra attention is given to the off-shell Higgs sample used in this thesis and two different kinds of re-weighting of the simulated events are applied in to produced an MC sample with wide mass spectrum way beyond the mass of Higgs ($\approx 125 \text{ GeV}$). We use the gluon fusion Higgs (ggH) sample to illustrate the procedures. The same procedures are applied to the VBF samples as well.

We start by generating separate samples with different Higgs pole mass. This is the mass of Higgs that appears in the propagator on the R.H.S of Eq. 1 as mentioned before. The raw distribution of the true mass in different samples (without any weight) is shown in Fig. 4 (left). As expected, the peak of the distribution moves to the right as the mass of the sample becomes larger, at the same time, the ‘peak’ of samples with very large mass is wider because the width of the Higgs increases. We also see that for some lower mass samples (200, 300, 400 GeV etc.), they have a cut-off (due to insufficient statistics) beyond $M \approx 2500 \text{ GeV}$ which means they have 0 statistics beyond that mass range. After applying the GEN, PU, and ME weights given by their individual MC process and JHUGen MELA, as shown in Fig. 4, we see that they are consistent with each others’ line shape. However, it is clear that:

- (i) Lower mass samples have insufficient statistics in the tail region

- (ii) Samples have poor statistics in mass windows that are far from their true mass (as listed in the legend).

The second point is best illustrated by the wide spikes of lower mass samples near their ‘cut-offs’, as well as the visible fluctuations of high-mass samples in the mass region (don’t let the visual mislead you, the plots are in semi-log scale).

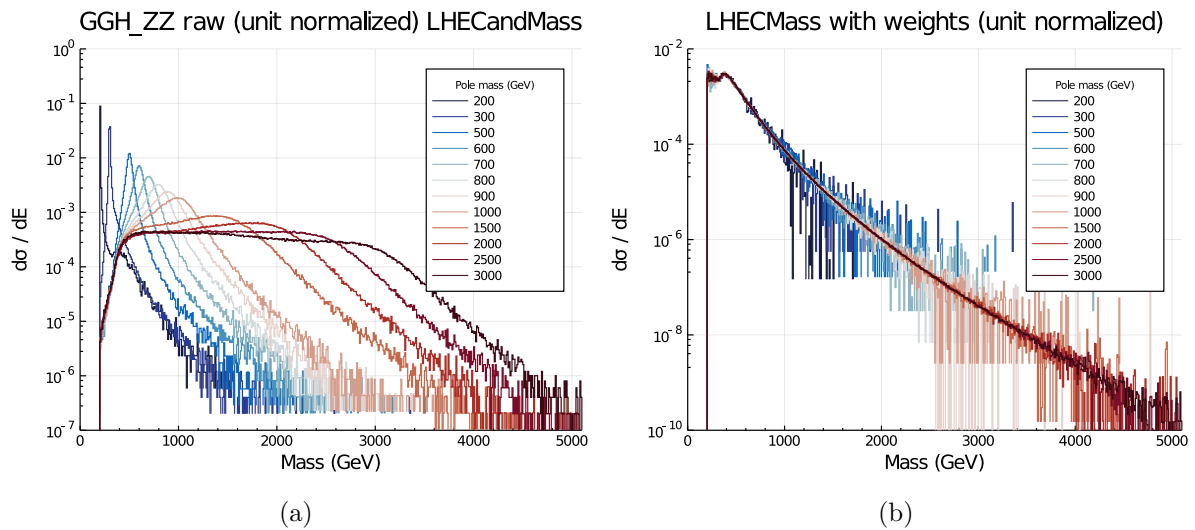


Figure 4: Unit normalized distributions of LHECandMass before (left) and after (right) applying the weights. Together they show a need to combine samples for a wide-range, high statistics signal sample. Bin size = 10 GeV.

The goal of the combination of samples is to use all the events, but with a correction weight such that each sample has a higher weight in the region where they pose good statistics while the overall normalization stays unchanged. To do this, we pick a list of ‘mass windows’ with edges sitting on the true masses of the samples, and we define effective number of events $N_{\text{eff}} = \frac{(\sum \text{wgts})^2}{\sum (\text{wgts}^2)}$ within each mass window. Here, the weight corresponds to the product of PU wgt, GEN wgt, K-factor, and ME weight for the GGH sample into consideration. For a specific GGH sample, i_0 and its events fall in a mass

window j , $N_{\text{eff}}^{i_0 j}$ is first obtained and a re-weighting factor can be computed:

$$\text{wgt}_{\text{window}}^{i_0 j} = \frac{N_{\text{eff}}^{i_0 j}}{\sum_i N_{\text{eff}}^{ij}} \quad (5)$$

This factor is applied to all events from sample i_0 within the window j . Conceptually, the effective number of events ensures the weight is not skewed by the difference in the overall normalization of samples, and in each of the mass windows, samples with more concentrated statistics in that window are given a higher weight. In Fig. 5 (a), a clear diagonal pattern can be seen. Physically it means that samples with higher true mass is given a higher weight in tail mass windows — consistent with the expected outcome. Complete table of weights can be found in Appendix A.1.

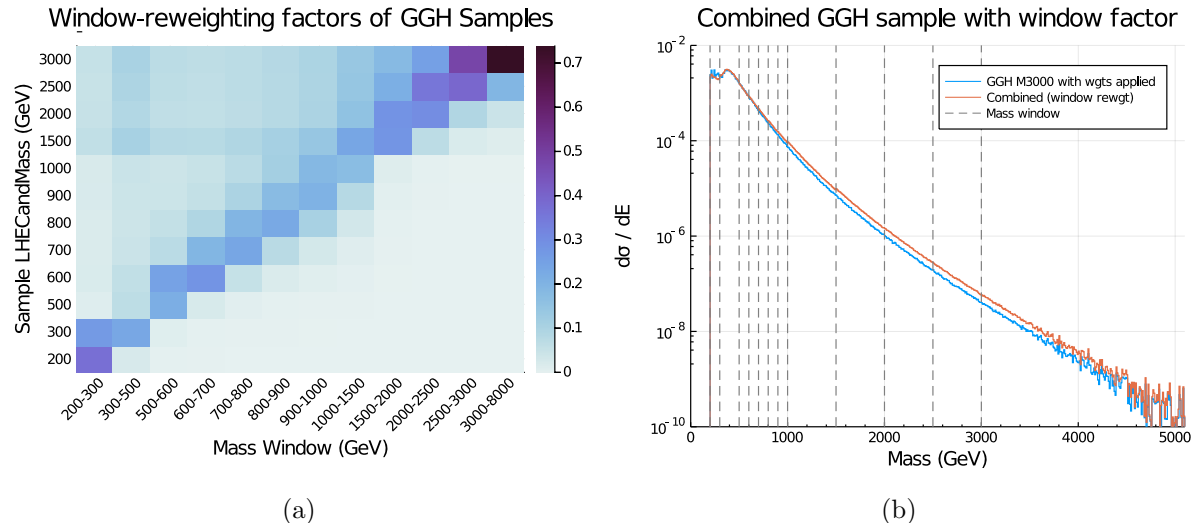


Figure 5: Heatmap of window re-weight factors of different samples and mass windows (left); effects of applying window factors for the combined sample (right)

However, even with the unit normalization, there are still inconsistency in the shape, as shown in Fig. 5 (b). This inconsistency is likely caused by the finite number of events and non-infinitesimal mass window size used. We introduce another correction factor for

this small artifacts. Iteratively going through every sample, between the previous and the next one, we derive a sample mass factor based on:

$$\text{wgt}_{\text{mass}}^{i,i+1} = \frac{\sum \text{wgt}_i}{\sum \text{wgt}_{i+1}}, \text{ for events that has Mass between sample mass of } i \text{ and } i + 1 \quad (6)$$

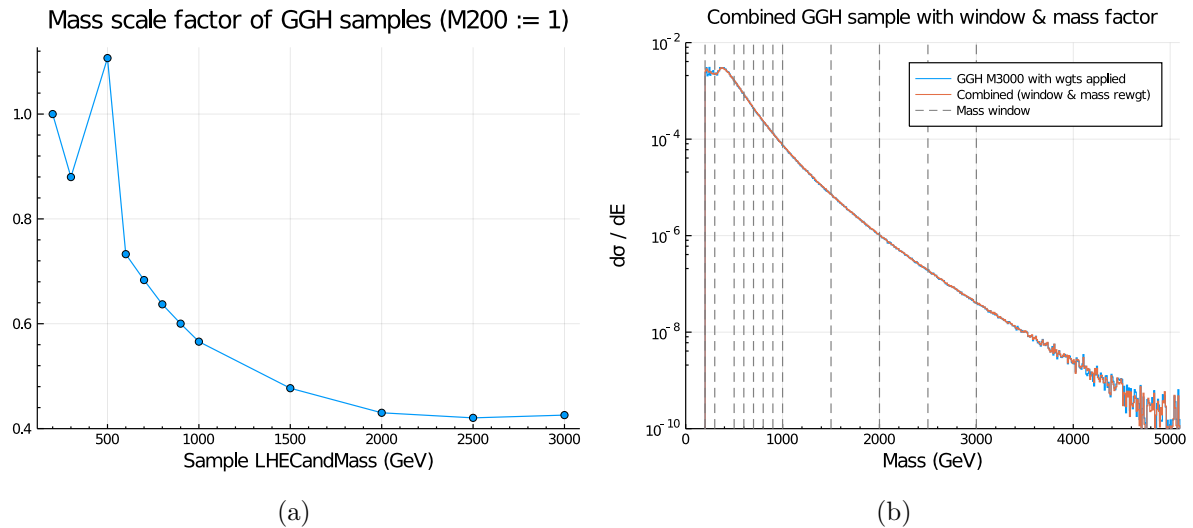


Figure 6: Iterative sample mass factors obtained (left) and the final combined sample (right)

This factor corrects the high variations of overall normalizations between samples. The factors and results are shown in Fig. 6. As expected, high mass samples need a down correction (not by a lot) to eliminate the deviated trend before. Complete tables of these weights for both samples can be found in Appendix A.2.

Finally, 1.10 is multiplied to the weights of all ggZZ processes (all of BKG, SIG, BSI of GGH sample) as a K factor for Next-to-next-to-leading-order (NNLO) \rightarrow Next-to-next-to-next-to-leading-order (N3LO) QCD.

Although we used the particular matrix element weights for one of the signal hypothesis, these two correction factors apply to all hypothesis. A plot of them without unit area normalization is shown in Fig. 7. As expected, the background exceeds the signal

by more than 100% which is partially why the constrain is hard to obtain.

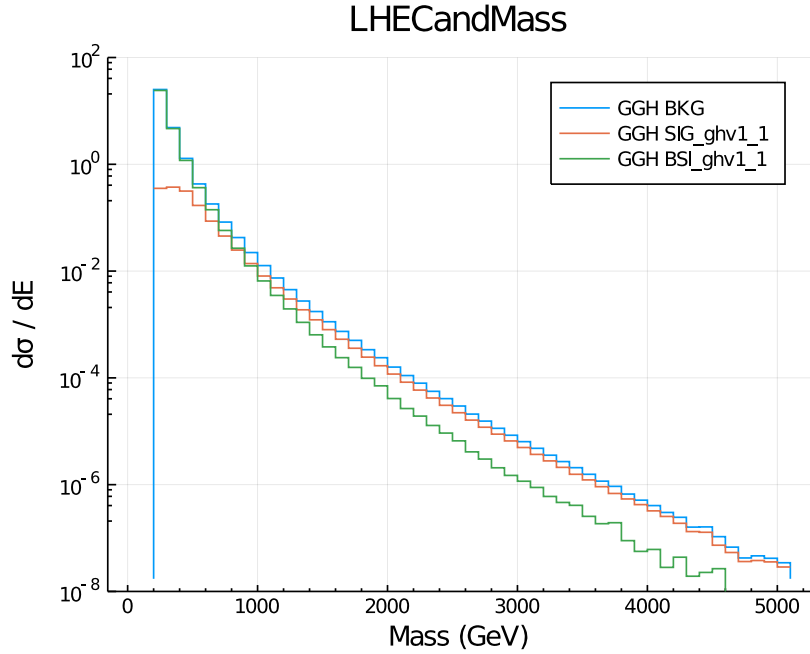


Figure 7: Distributions of background, signal, and background signal interaction

2.3 Strategy in variable selection and binning and systematical uncertainties

After we prepared the signal samples and decided on the event selection criteria, we then decided on the variables and their (2D histogram, as shown in Fig. 9) ‘binning’ before a combined-limits fit can be applied. As discussed in earlier sections, one of the more inventive variables newly introduced specifically for the analysis is the DJJVBF discriminator. However, it is clear that this variable is undefined for events with $N_{\text{jets}} < 2$. To not ‘waste’ any statistical significance, we use E_T^{miss} in its place for the $N_{\text{jets}} = 0, 1$ categories. In total, we have 2 (ee or $\mu\mu$) $\times 4$ ($N_{\text{jets}} = 0, 1, 2, 3+$) $= 8$ channels to consider when making histogram templates. The bin edges for different categories in number of jets is the following:

- $N_{\text{jets}} \geq 2$
 - $M_T^{\text{ZZ}} = 150, 300, 400, 600, 800, 1000, 13000$ (GeV)
 - $\text{KD1} = \text{DJJVBF} = 0, 0.2, 0.4, 0.6, 0.8, 1$
- $N_{\text{jets}} < 2$
 - $M_T^{\text{ZZ}} = 150, 300, 400, 600, 800, 1000, 13000$ (GeV)
 - $\text{KD1} = E_T^{\text{miss}} = 125, 200, 280, 420, 500, 800, 13000$ (GeV)

The higher mass (M_T^{ZZ}) bins are wider because samples have difficulty filling them due to physical reasons (especially for backgrounds) and because the cuts are applied.

The different shapes of backgrounds and signals are shown in Fig. 8. These plots have noticeable features including the VBF samples peak at ends of the D_{jj}^{VBF} showing the power of this variable. See Appendix B.1 for a more complete collection of plots.

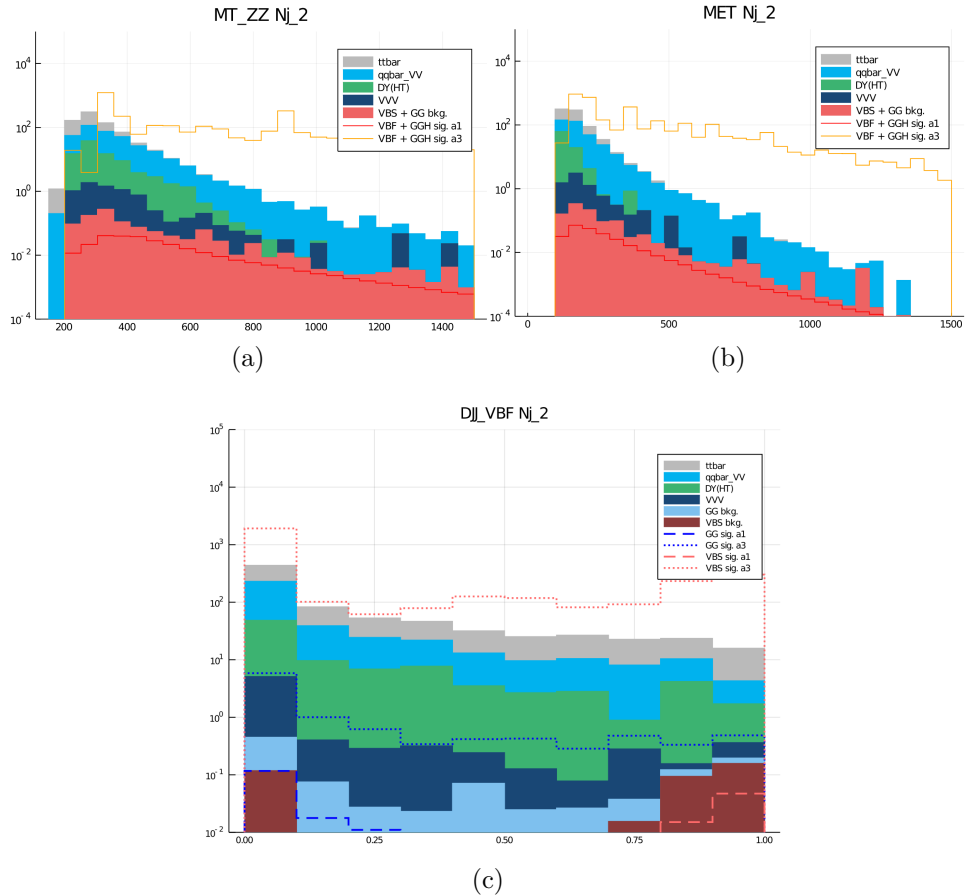


Figure 8: Distribution (integral not to be taken literal) of M_T^{ZZ} (left), E_T^{miss} (right), and D_{jj}^{VBF} (bottom) for backgrounds and signals with $N_{\text{jets}} = 2$. Here sig a3 is a scaled up version of the signal (a1) and VVV corresponds to WWW or WWZ or WZZ

We use the above binning for all samples and 8 channels that are considered in this thesis. A limited number of the 2d template histograms are shown in Fig. 9. Again, we notice the peaks of D_{jj}^{VBF} in VBF samples match our expectation. See Appendix B.3 for a compilation of template histograms of ggZZ sample.

For low-yield background samples, due to the nature of NLO samples, bins sometimes will have negative content. To mitigate its effect on the likelihood fitting (pathological), we replace the bin content by $(\text{Integral of the histogram}) \times 10^{-5}$.

Systematical uncertainties are also included in the fitting:

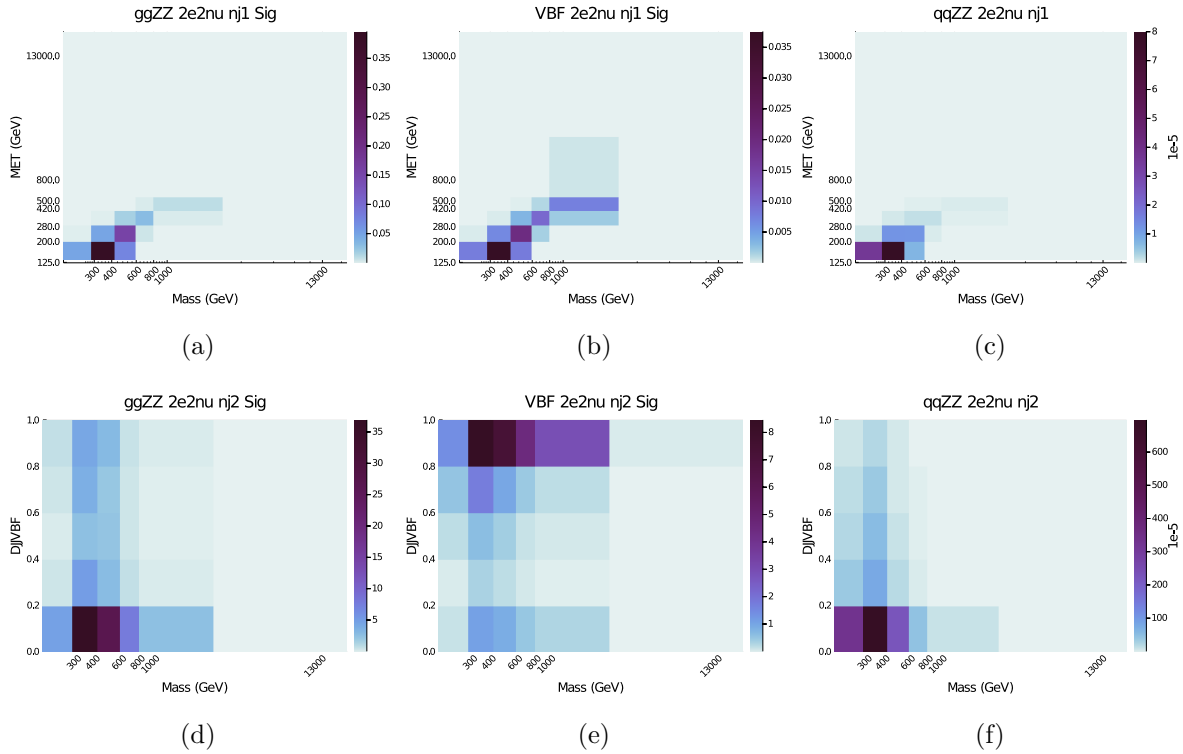


Figure 9: ggZZ (left), VBF (center), and qqZZ (right), histogram templates for fitting, in $2e2\nu$ channel with 1,2 jet(s). Color bar (event counts) is scaled by 1×10^5 .

- Luminosities GGH_ZZ, VBF_ZZ, qqZZ, qqWZ
- NRB (non-resonant background) Estimation: TT, WW
- Branching Ratio of Higgs to ZZ to 4l: GGH_ZZ, VBF_ZZ
- K-fatcors of background gluongluon parameter

See Table. 1.5 for respective range of these uncertainties.

Chapter 3

Results and interpretation

Final results of this thesis are presented. The ‘expected’ limits are interpreted.

3.1 Limits on Higgs decay width

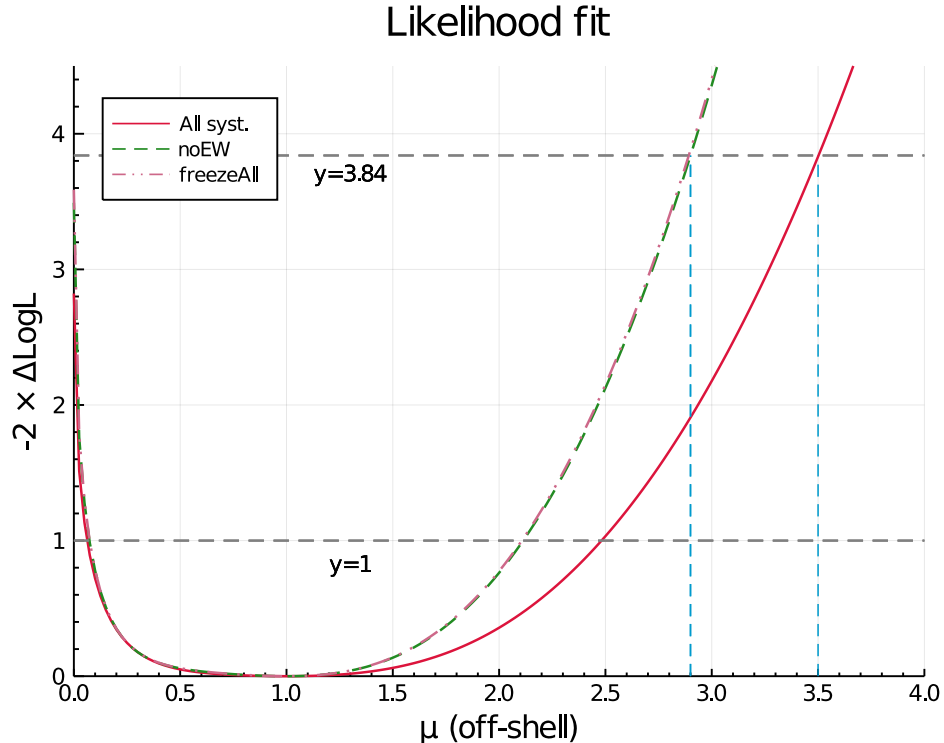


Figure 10: Maximum likelihood fit of $\mu_{\text{off-shell}}^H$ (off-shell rate ratio). For all systematics (red), no Electroweak syst. (green), 0 syst. (orange): y -intersect= $\{2.82, 3.49, 3.59\}$, 1σ lower limits= $\{0.075, 0.075, 0.075\}$, 1σ higher limits= $\{2.45, 2.13, 2.1\}$, 95% CL limits= $\{3.5, 2.9, 2.9\}$, respectively.

After running through Combined Limited tool [20, 21, 22] for likelihood fitting, we first extract the significance of the off-shell rate. (Fig. 10) The y-axis is understood to be σ^2 in terms of significance. Thus the intersection with the y-axis is the signal sensitivity. In other words, rejection of the 0 width hypothesis (no off-shell) has a significance of $\sqrt{1.61} \approx 1.26\sigma$ in this fit with all the systematic uncertainties included. As the systematics are ‘turned off’, the constraint becomes tighter, producing an error band for the expected final result in the upcoming official analysis. The electroweak uncertainty is displayed individually as it encompasses most of the systematic uncertainties.

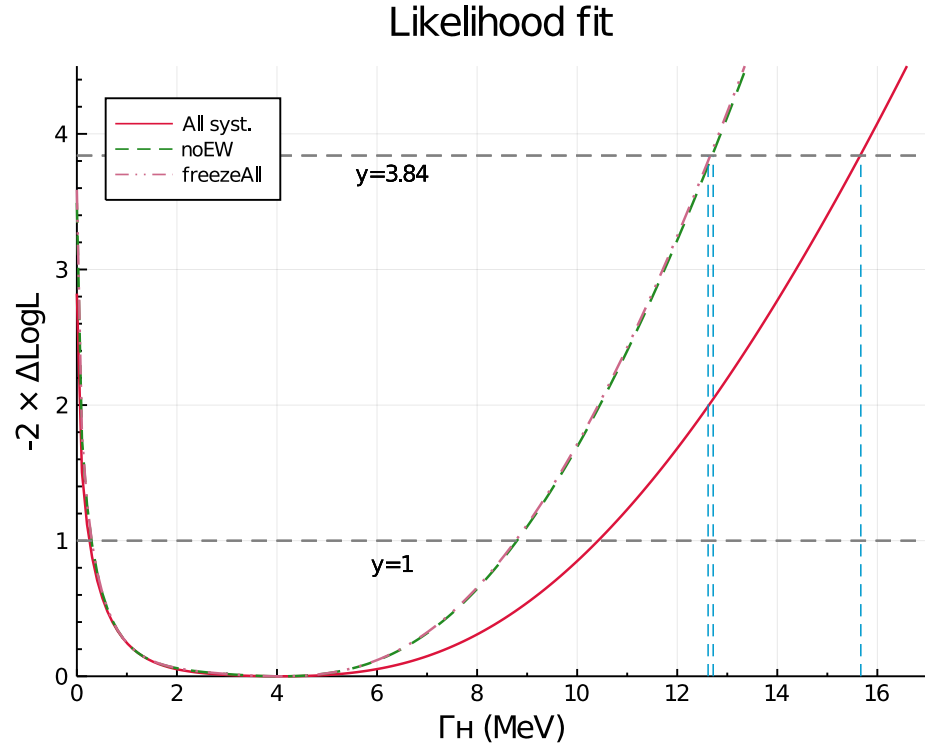


Figure 11: Maximum likelihood fit of Higgs decay width. For all systematics (red), no Electroweak syst. (green), 0 syst. (orange): $y\text{-intersect}=\{2.82, 3.49, 3.59\}$, 1σ lower limits= $\{0.20, 0.31, 0.31\}$ MeV, 1σ higher limits= $\{10.38, 8.75, 8.65\}$ MeV, 95% CL limits= $\{15.67, 12.72, 12.62\}$ MeV, respectively.

Furthermore, by un-constraining the μ_F and μ_V , which are the production rate of Higgs from fermion fusion vs. massive boson fusion as mentioned in the Eqn. 1, we can obtain the limit on the Γ_H itself. We adopt the range suggested [23] for these two systematics. The constraint on the decay width of Higgs Γ_H is shown in Fig. 11. The minimal (max likelihood) falls on 4.07 MeV, which is consistent with the standard model hypothesis. Again, 1σ and 95% CL are marked respectively. And a final result of $\Gamma_H < 16.38$ MeV 95% CL can be quoted.

Appendix A

Weights table for Higgs sample

A.1 Windowed re-weighting results

(100 GeV)	2-3	3-5	5-6	6-7	7-8	8-9	9-10	10-15	15-20	20-25	25-30	30-80
30	0.0572	0.1082	0.0737	0.0686	0.0742	0.0857	0.1015	0.1431	0.1832	0.2573	0.4859	0.74
25	0.0531	0.1011	0.071	0.0659	0.0734	0.083	0.1001	0.1461	0.2169	0.3597	0.3971	0.1964
20	0.0545	0.0913	0.0659	0.0633	0.0713	0.084	0.1021	0.1599	0.2889	0.3043	0.0933	0.0481
15	0.0643	0.1118	0.0829	0.0812	0.0948	0.113	0.1447	0.2395	0.2847	0.0732	0.022	0.0141
10	0.0242	0.0493	0.044	0.0529	0.0752	0.1179	0.1896	0.1752	0.0141	0.0028	0.0008	0.0008
9	0.0238	0.0468	0.0465	0.0602	0.1028	0.1791	0.2064	0.0832	0.0066	0.0013	0.0004	0.0003
8	0.0205	0.045	0.0592	0.0941	0.1991	0.2324	0.1099	0.0341	0.0031	0.0007	0.0002	0.0001
7	0.0207	0.0478	0.076	0.1965	0.2409	0.0787	0.0324	0.012	0.0014	0.0003	0.0001	0.0001
6	0.0212	0.0637	0.2502	0.2875	0.0573	0.0205	0.0098	0.0048	0.0007	0.0002	0.0	0.0001
5	0.014	0.0705	0.217	0.0251	0.0083	0.0041	0.0023	0.0014	0.0002	0.0	0.0	0.0
3	0.2708	0.2386	0.0111	0.0037	0.002	0.0012	0.0008	0.0006	0.0001	0.0	0.0	0.0
2	0.3757	0.0259	0.0026	0.001	0.0006	0.0004	0.0003	0.0001	0.0	0.0	0.0	0.0

Table 3: Windowed re-weighting result for ggZZ samples.

(100 GeV)	2-3	3-4	4-5	5-6	6-7	7-8	8-9	9-10	10-15	15-20	20-25	25-30	30-80
30	0.0013	0.0024	0.0021	0.0035	0.003	0.005	0.01	0.0112	0.0265	0.0764	0.1583	0.3873	0.6233
25	0.0017	0.0028	0.0023	0.0046	0.004	0.0063	0.0121	0.0149	0.039	0.1193	0.2795	0.3844	0.2218
20	0.0015	0.0044	0.0038	0.0067	0.0065	0.0096	0.0211	0.0256	0.0709	0.2562	0.3658	0.1491	0.0904
15	0.0045	0.0088	0.0075	0.015	0.0131	0.0218	0.0448	0.06	0.1727	0.4011	0.1484	0.0569	0.0434
10	0.0052	0.0077	0.0092	0.0184	0.0208	0.0464	0.0152	0.0085	0.2471	0.0459	0.0136	0.0058	0.0055
9	0.0054	0.0142	0.0167	0.0378	0.0449	0.0975	0.332	0.4022	0.2029	0.0389	0.0122	0.0058	0.0052
8	0.0107	0.0196	0.0252	0.0623	0.0998	0.3037	0.187	0.2898	0.1195	0.0255	0.0085	0.0036	0.0042
7	0.0087	0.0226	0.0299	0.1043	0.2057	0.2715	0.2067	0.0905	0.0481	0.0125	0.0047	0.0023	0.0022
6	0.0176	0.0482	0.0882	0.0557	0.4805	0.157	0.1003	0.0499	0.0348	0.0108	0.0039	0.002	0.0017
5	0.029	0.1134	0.2939	0.5247	0.1041	0.0499	0.0397	0.025	0.0188	0.0065	0.0026	0.0015	0.0013
4	0.0634	0.336	0.4353	0.1231	0.001	0.0183	0.0174	0.0129	0.0111	0.0042	0.0015	0.0008	0.0007
3	0.1082	0.3288	0.0725	0.0305	0.0114	0.0086	0.009	0.0064	0.0058	0.0022	0.0009	0.0005	0.0004
2	0.7428	0.0912	0.0134	0.0132	0.005	0.0042	0.0047	0.0031	0.0028	0.0004	0.0	0.0	0.0

Table 4: Windowed re-weighting result for VBF samples.

A.2 Sample mass factors for ggZZ and VBF_ZZ samples

ggZZ		VBF_ZZ	
Mass (GeV)	Factor	Mass (GeV)	Factor
200	1	200	1
300	0.8798	300	0.8731
500	1.1068	400	0.7873
600	0.7327	500	0.7106
700	0.6833	600	0.6361
800	0.6370	700	0.5754
900	0.6001	800	0.5217
1000	0.5658	900	0.4818
1500	0.4769	1000	0.4257
2000	0.4300	1500	0.3255
2500	0.4204	2000	0.2968
3000	0.4256	2500	0.2898
		3000	0.2916

Table 5: Sample mass re-weighting factors for both signal samples.

Appendix B

Additional figures

B.1 1D Histograms of variables used for constructing 2d templates histograms

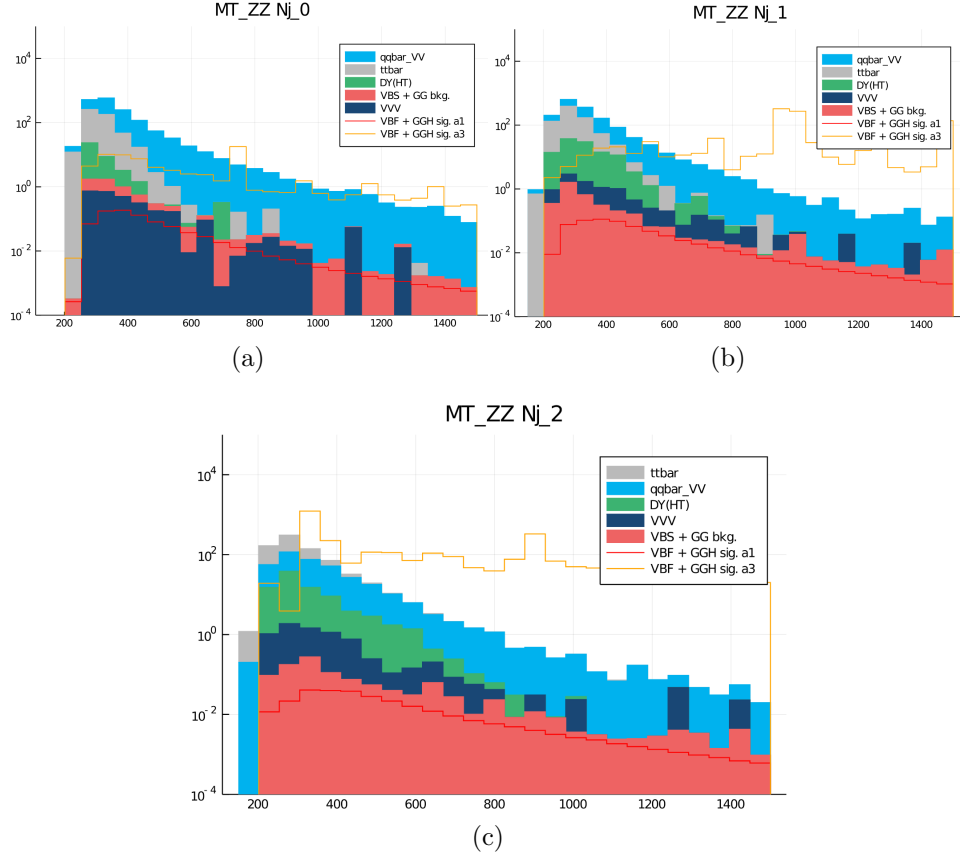


Figure 12: Distribution (integral not to be taken literal) of E_T^{miss} for backgrounds and signals with different N_{jets} . Here sig a3 is a scaled up version of the signal (a1) and VVV corresponds to WWW or WWZ or WZZ

B.2 Signal sample fitting template histogram of background and signal (z-axis scaled by 1×10^5)

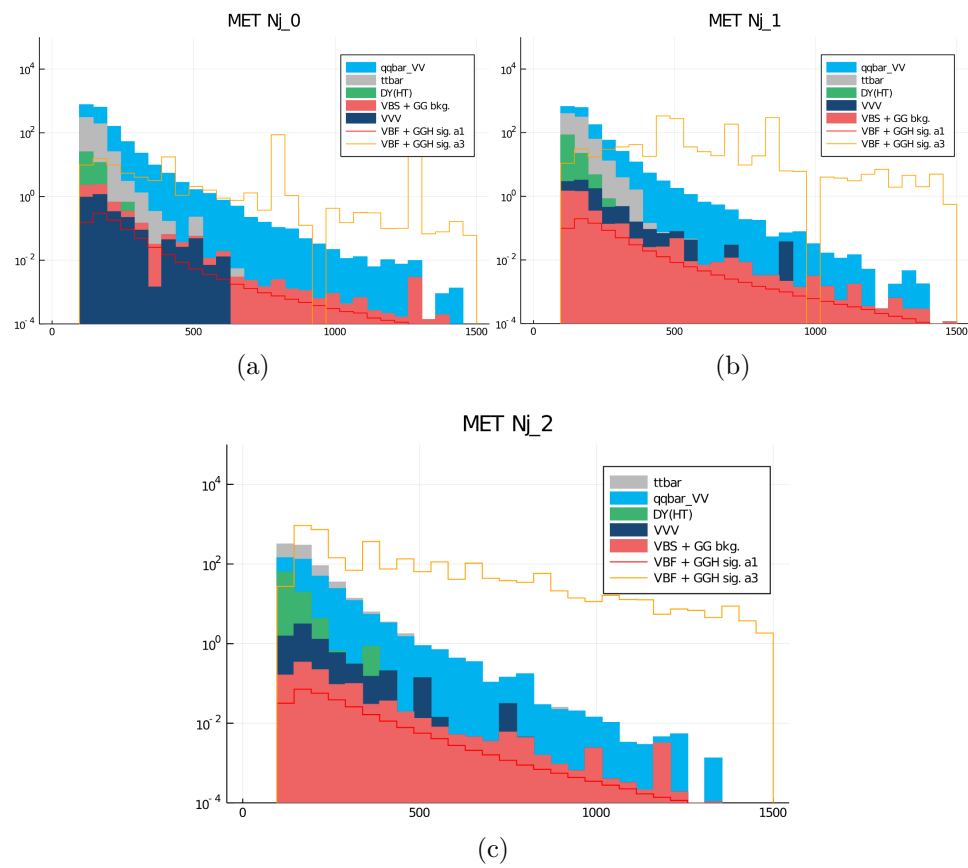


Figure 13: Distribution (integral not to be taken literal) of E_T^{miss} for backgrounds and signals with different N_{jets} . Here sig a3 is a scaled up version of the signal (a1) and VVV corresponds to WWW or WWZ or WZZ

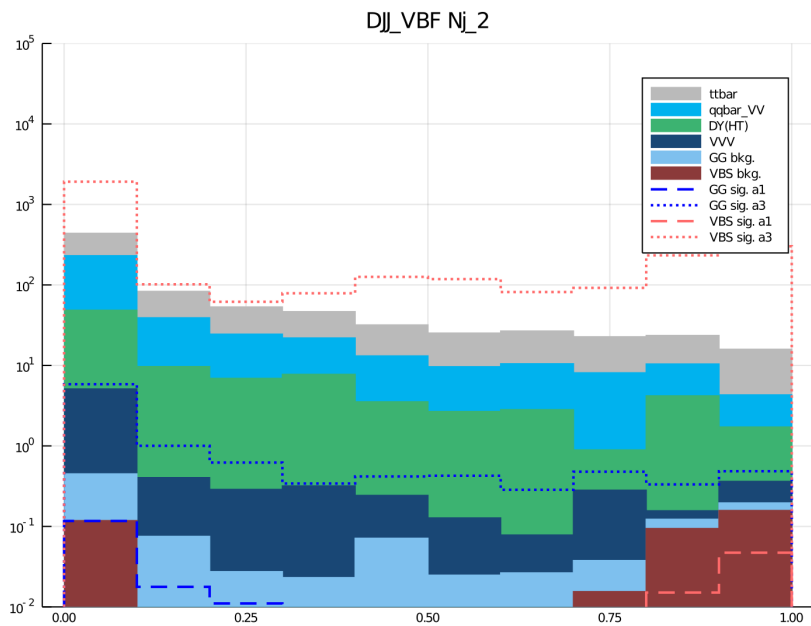
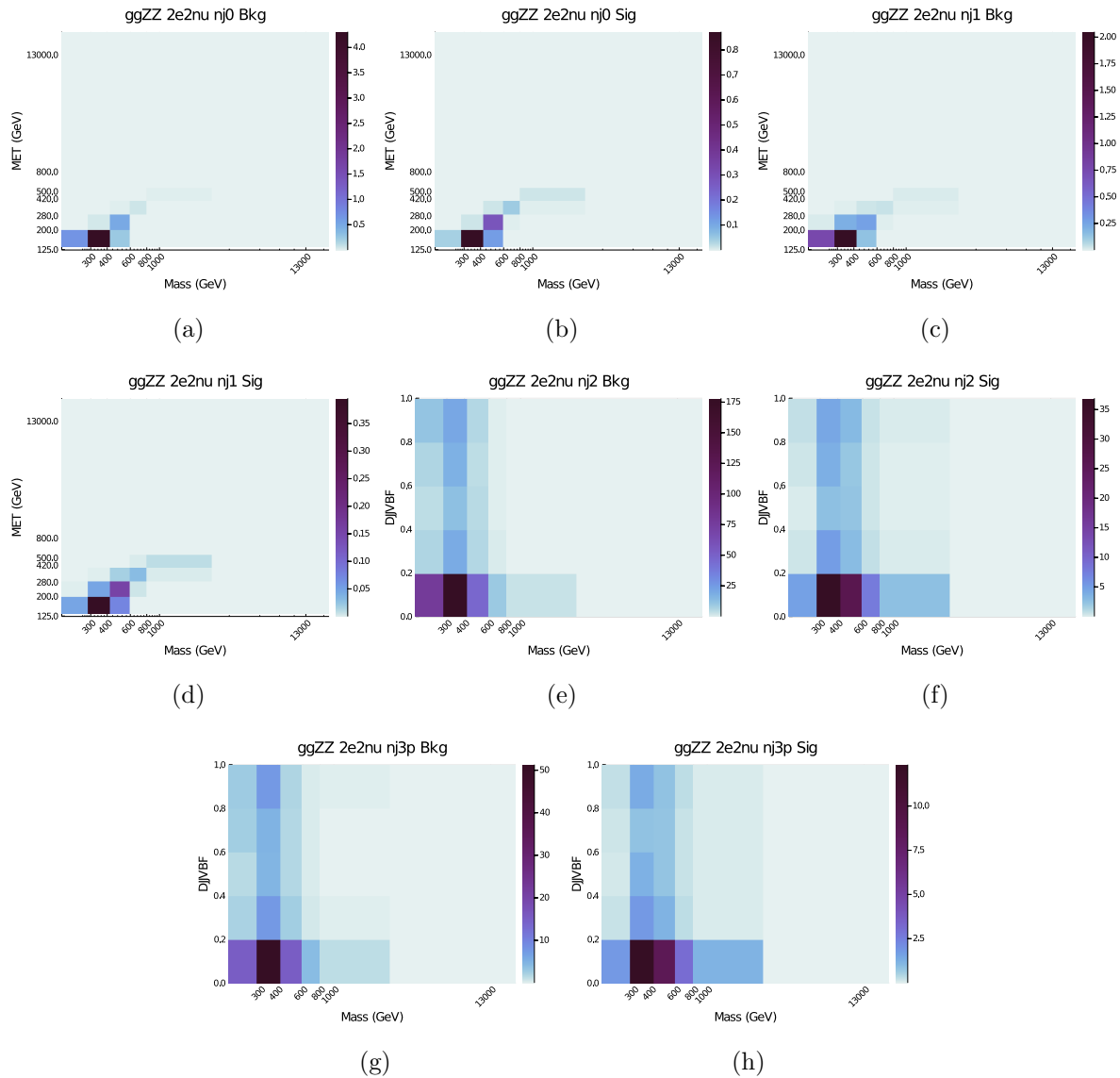
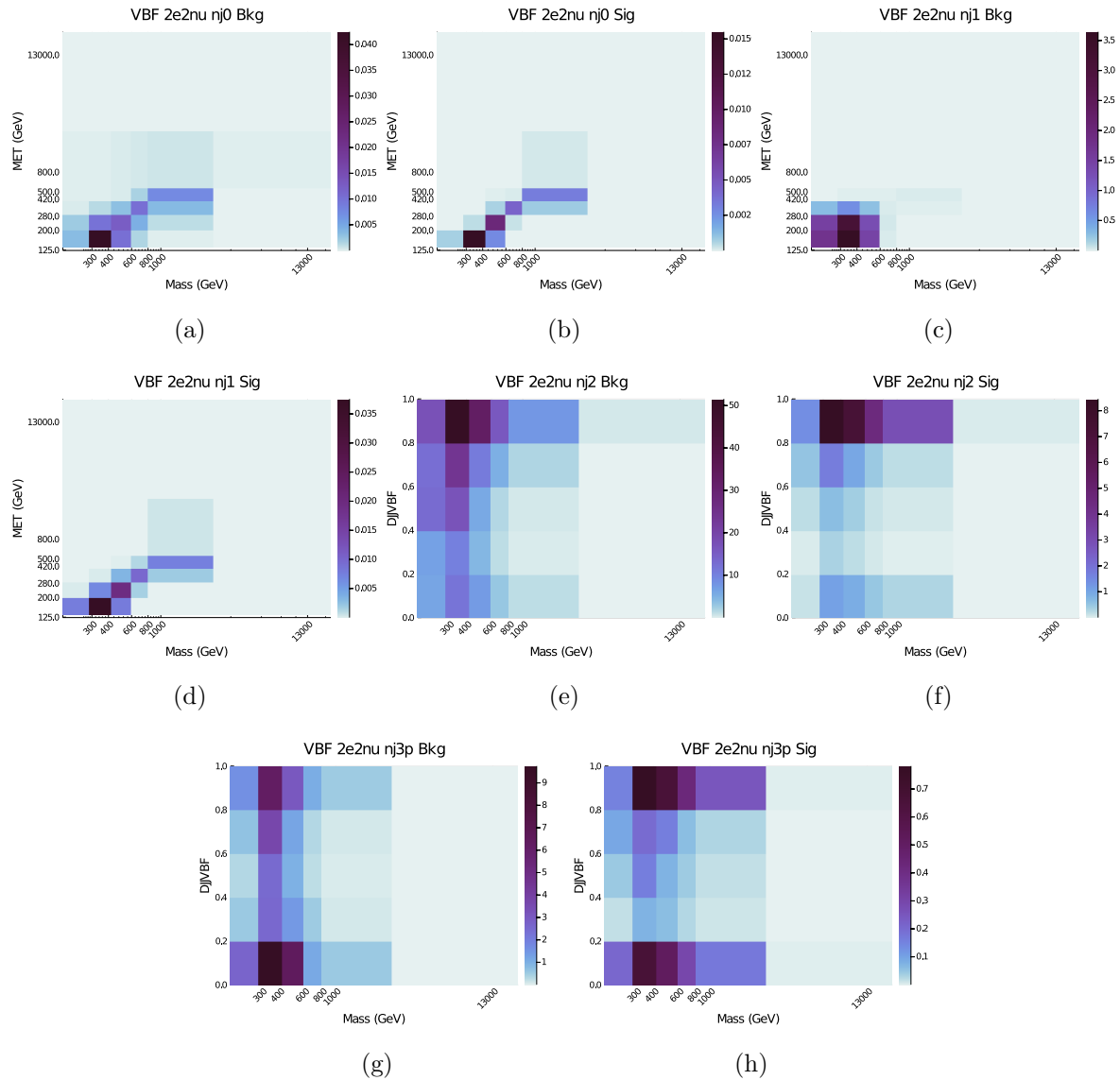
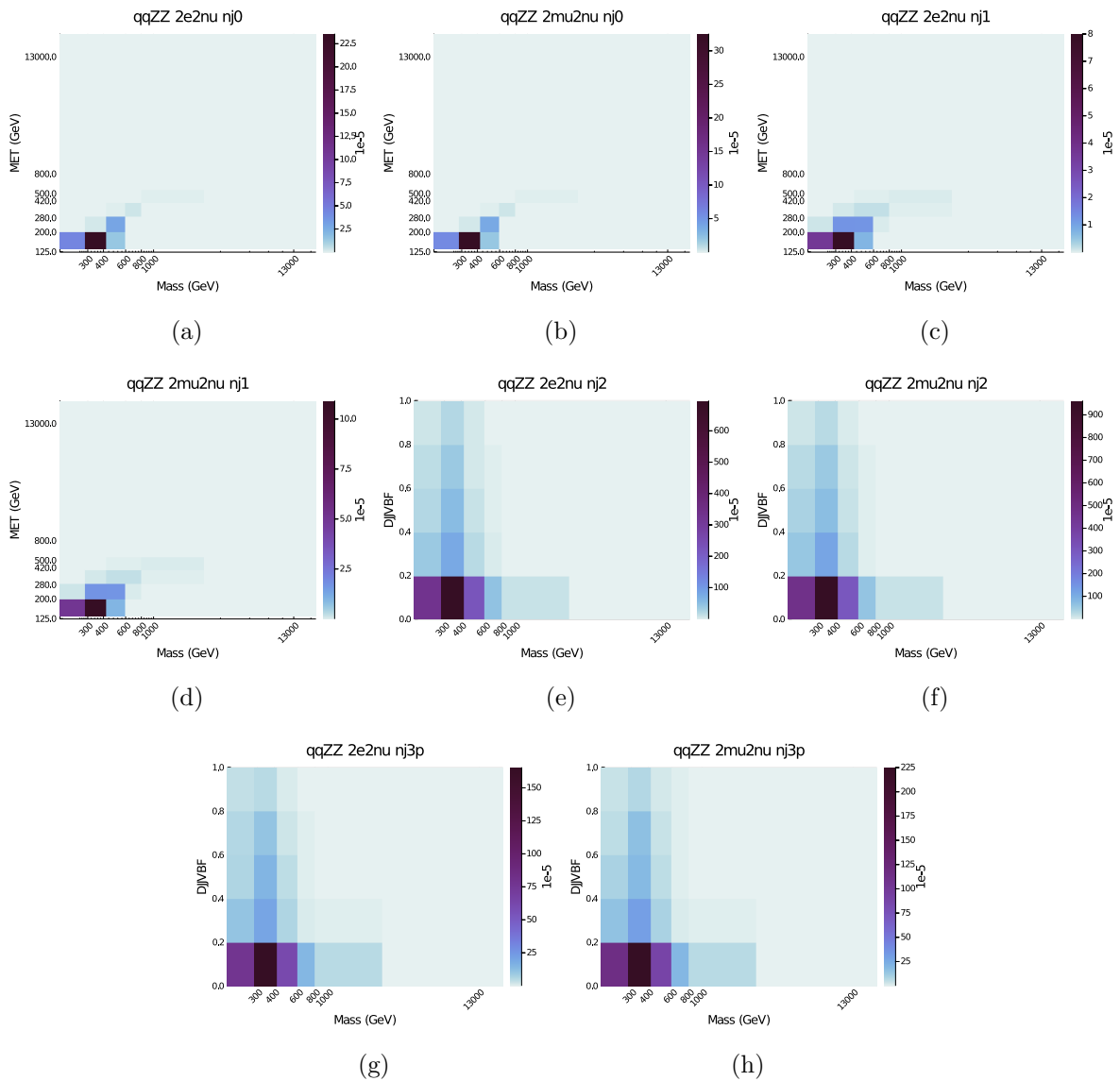


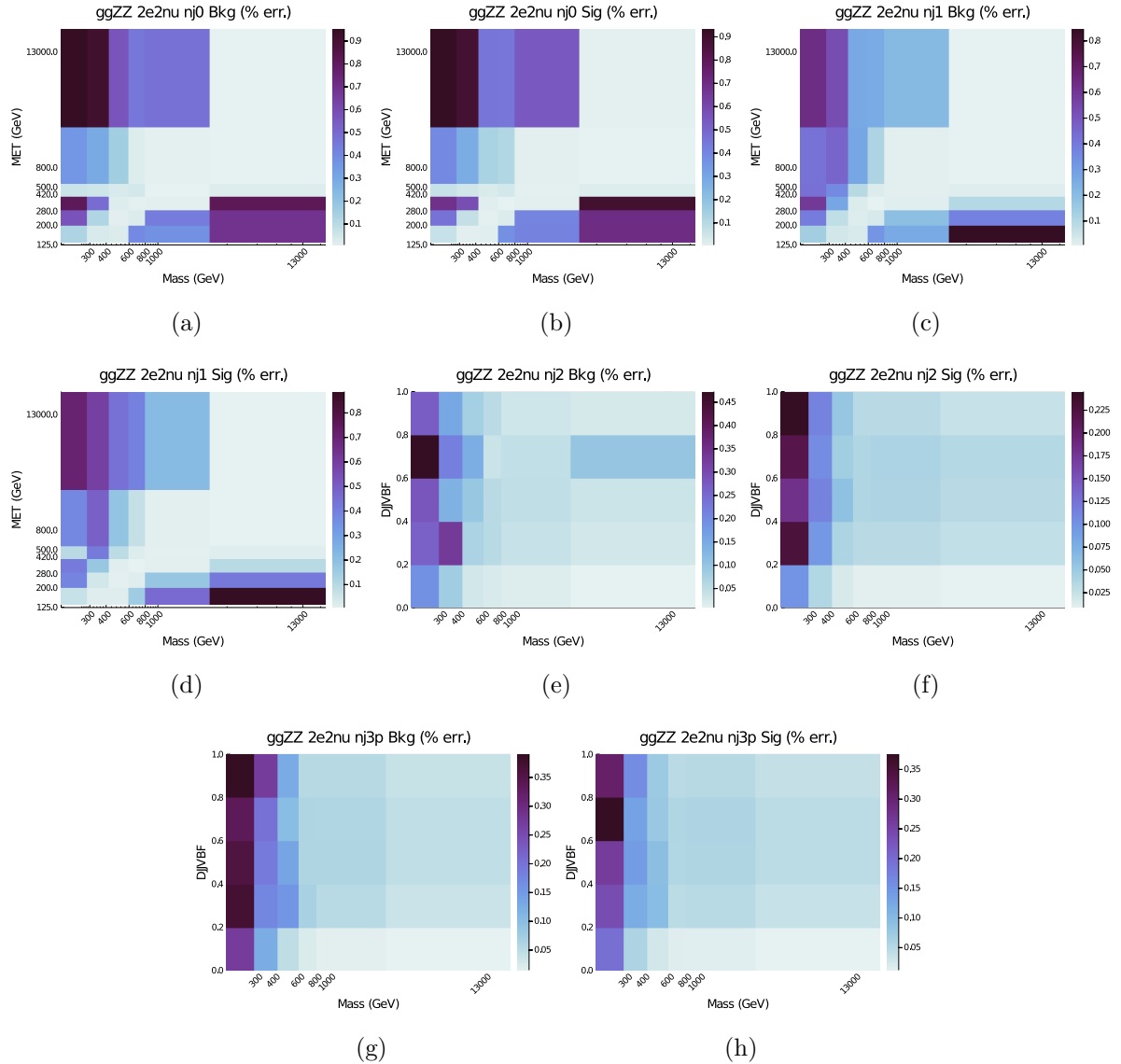
Figure 14: Distribution (integral not to be taken literal) of D_{jj}^{VBF} for backgrounds and signals with $N_{\text{jets}} = 2$. Here sig a3 is a scaled up version of the signal (a1) and VVV corresponds to WWW or WWZ or WZZ

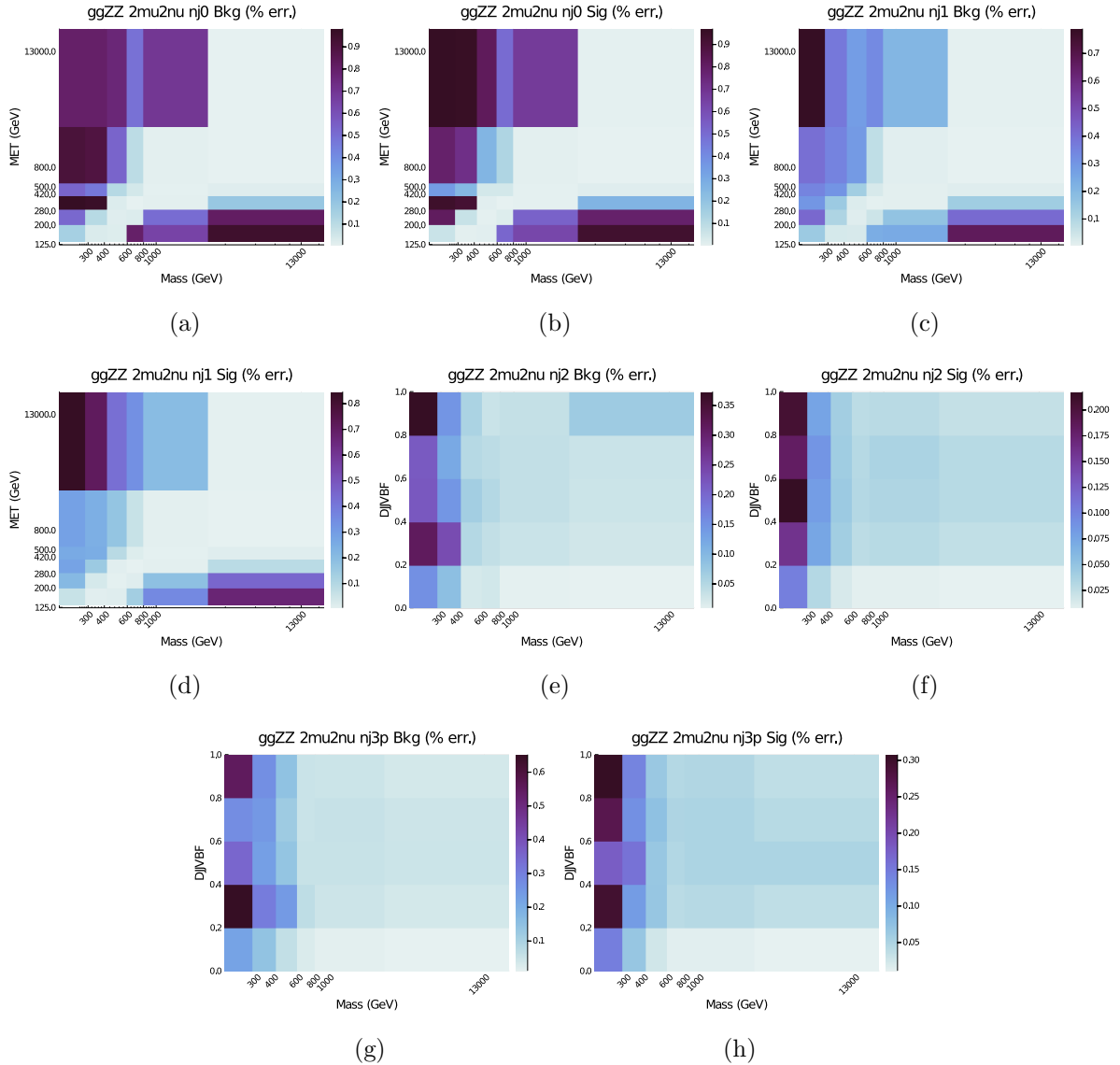


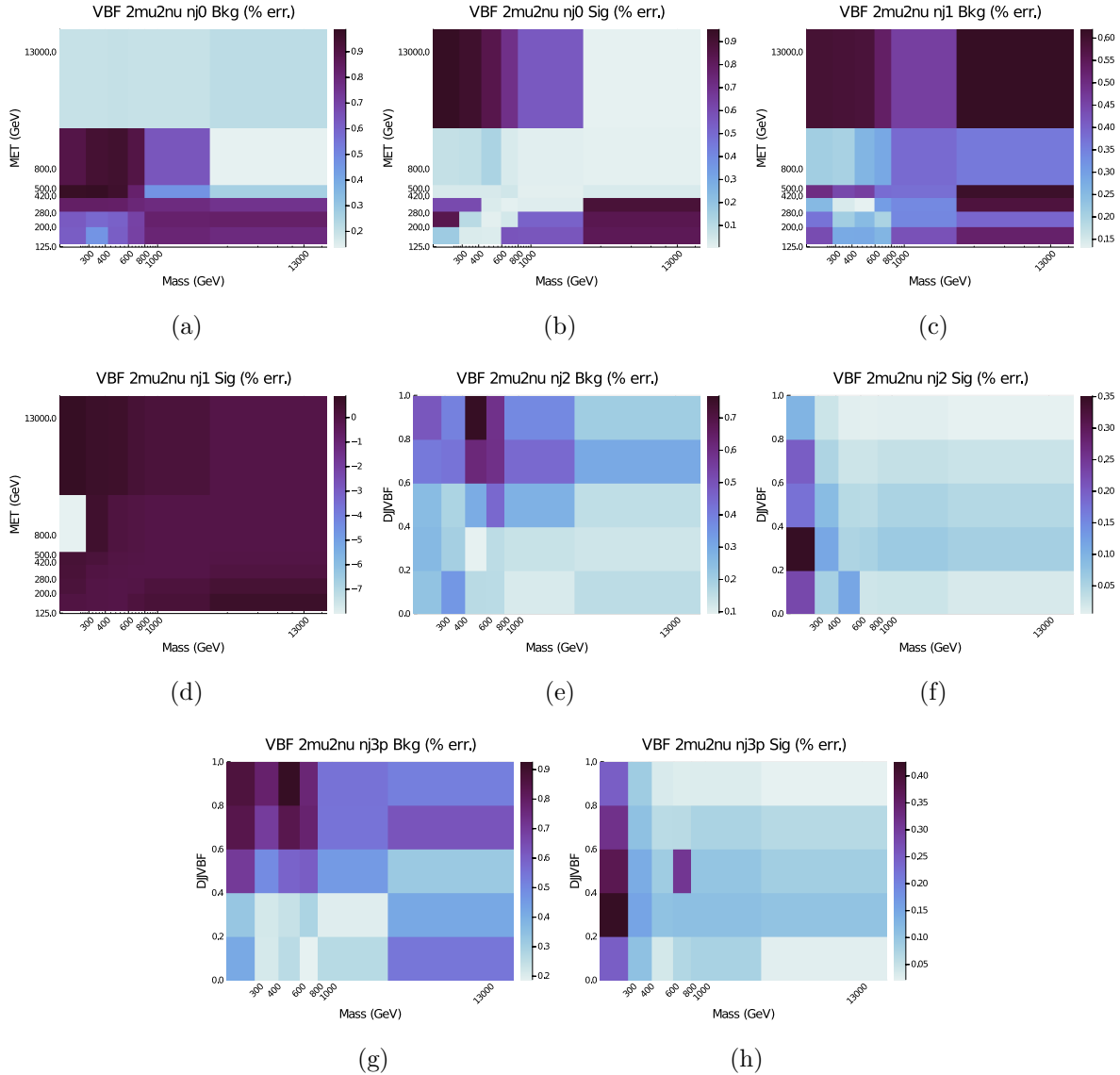


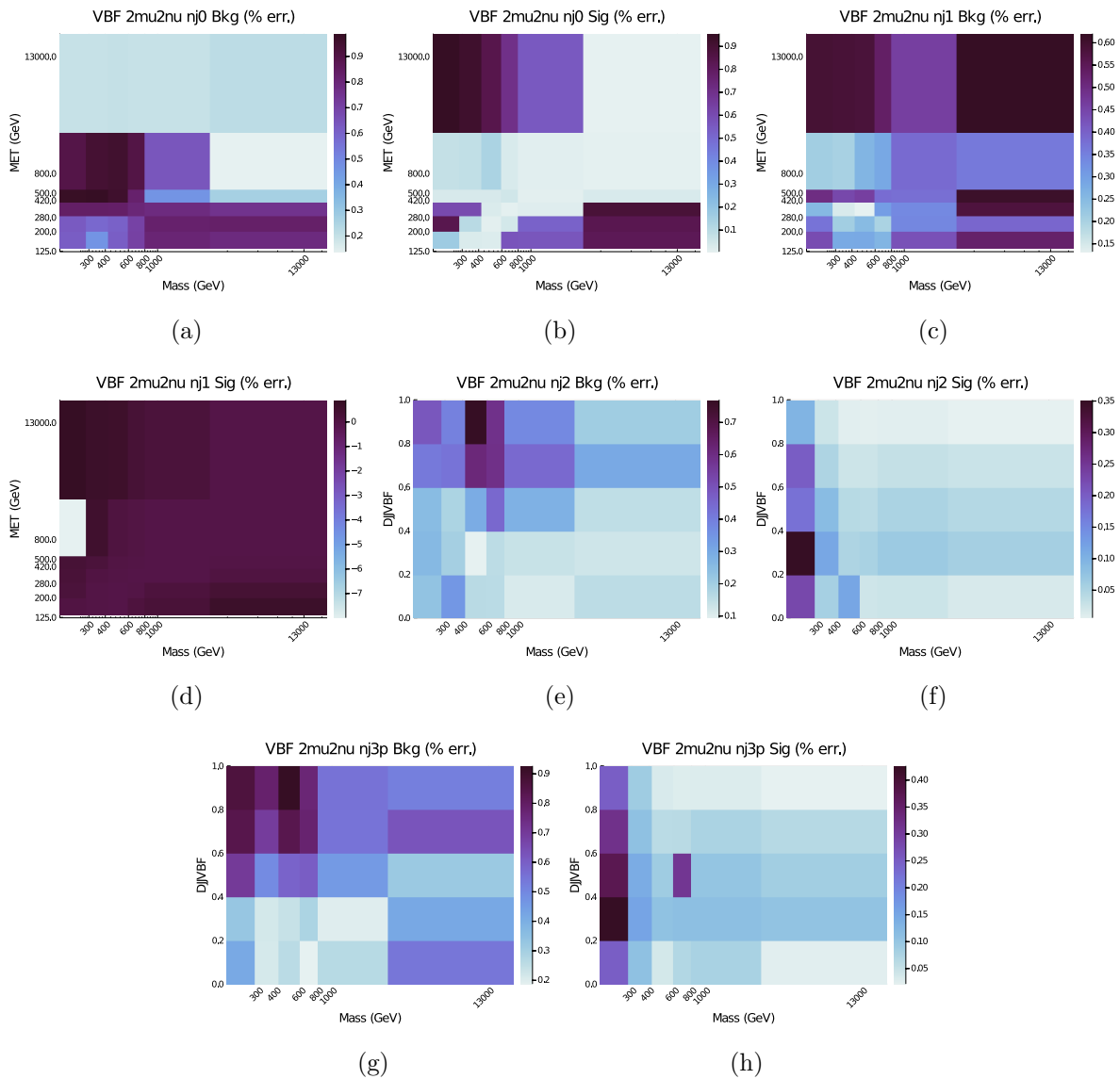


B.3 Signal sample fitting template histogram relative error of background and signal









Bibliography

- [1] “LumiPublicResults < CMSPublic < TWiki.”
<https://twiki.cern.ch/twiki/bin/view/CMSPublic/LumiPublicResults>.
- [2] Geant4 Collaboration, *Geant4—a simulation toolkit*, .
- [3] V. I. Klyukhin, N. Amapane, A. Ball, B. Curé, A. Gaddi, H. Gerwig, M. Mulders, V. Calvelli, A. Hervé, and R. Loveless, *Validation of the CMS magnetic field map*, arXiv:1606.0038.
- [4] CMS Collaboration, *Particle-flow reconstruction and global event description with the CMS detector*, arXiv:1706.0496.
- [5] “[0802.1189] the anti-k_t jet clustering algorithm.”
- [6] M. Cacciari, G. P. Salam, and G. Soyez, *FastJet user manual*, .
- [7] C. Collaboration, *Measurement of the properties of a higgs boson in the four-lepton final state*, arXiv:1312.5353.
- [8] N. Kauer and G. Passarino, *Inadequacy of zero-width approximation for a light higgs boson signal*, .
- [9] J. M. Campbell, R. K. Ellis, and C. Williams, *Bounding the higgs width at the LHC using full analytic results for $gg \rightarrow e^-e^+ - +$* , .
- [10] U. Sarica, *Measurements of Higgs Boson Properties in Proton-Proton Collisions at $\sqrt{s} = 7, 8$ and 13 TeV at the CERN Large Hadron Collider*. Springer Theses. Springer International Publishing.
- [11] P. Nason and G. Zanderighi, *W+W-, WZ and ZZ production in the POWHEG-BOX-v2*, .
- [12] A. V. Gritsan, J. Roskes, U. Sarica, M. Schulze, M. Xiao, and Y. Zhou, *New features in the JHU generator framework*, arXiv:2002.0988.

- [13] J. Alwall, R. Frederix, S. Frixione, V. Hirschi, F. Maltoni, O. Mattelaer, H.-S. Shao, T. Stelzer, P. Torrielli, and M. Zaro, *The automated computation of tree-level and next-to-leading order differential cross sections, and their matching to parton shower simulations*, .
- [14] P. Skands, S. Carrazza, and J. Rojo, *Tuning PYTHIA 8.1: the monash 2013 tune*, .
- [15] T. N. Collaboration, R. D. Ball, V. Bertone, S. Carrazza, L. Del Debbio, S. Forte, P. Groth-Merrild, A. Guffanti, N. P. Hartland, Z. Kassabov, J. I. Latorre, E. R. Nocera, J. Rojo, L. Rottoli, E. Slade, and M. Ubiali, *Parton distributions from high-precision collider data*, arXiv:1706.0042.
- [16] J. M. Campbell, R. K. Ellis, M. Czakon, and S. Kirchner, *Two loop correction to interference in $gg \rightarrow ZZ$* , .
- [17] F. Caola, K. Melnikov, R. Röntsch, and L. Tancredi, *QCD corrections to ZZ production in gluon fusion at the LHC*, . Publisher: American Physical Society.
- [18] CMS Collaboration, *Identification of heavy-flavour jets with the CMS detector in pp collisions at 13 TeV*, arXiv:1712.0715.
- [19] C. Collaboration, *Search for a higgs boson in the mass range from 145 to 1000 GeV decaying to a pair of w or z bosons*, arXiv:1504.0093.
- [20] ATLAS and C. M. S. Collaborations, *Measurements of the higgs boson production and decay rates and constraints on its couplings from a combined ATLAS and CMS analysis of the LHC \sqrt{s} collision data at $\sqrt{s} = 7$ and 8 TeV*, arXiv:1606.0226.
- [21] “Procedure for the LHC higgs boson search combination in summer 2011.” Institution: CERN-CMS-NOTE-2011-005 Library Catalog: cds.cern.ch Number: ATL-PHYS-PUB-2011-011.
- [22] “[1103.0354] incorporating nuisance parameters in likelihoods for multisource spectra.”
- [23] “Measurements of properties of the higgs boson in the four-lepton final state in proton-proton collisions at $\sqrt{s} = 13\text{TeV}$.” Library Catalog: cds.cern.ch Number: CMS-PAS-HIG-19-001.